Nano Research
DOI 10.1007/s12274-014-0605-x
Research Article
ISSN 1998-0124
CN 11-5974/O4

Multifunctional Ultrasmall Pd Nanosheets for Enhanced Near-Infrared Photothermal Therapy and Chemotherapy of Cancer

Shaoheng Tang, Mei Chen, and Nanfeng Zheng (✉)

Nano Res., **Just Accepted Manuscript** • DOI: 10.1007/s12274-014-0605-x
http://www.thenanoresearch.com on October 8 2014

Just Accepted

TSINGHUA UNIVERSITY PRESS Springer

TABLE OF CONTENTS (TOC)

Multifunctional Ultrasmall Pd Nanosheets for Enhanced Near-Infrared Photothermal Therapy and Chemotherapy of Cancer

Shaoheng Tang, Mei Chen and Nanfeng Zheng*

State Key Laboratory for Physical Chemistry of Solid Surfaces, Collaborative Innovation Center of Chemistry for Energy Materials, and Department of Chemistry, College of Chemistry and Chemical Engineering, Xiamen University, Xiamen 361005, China

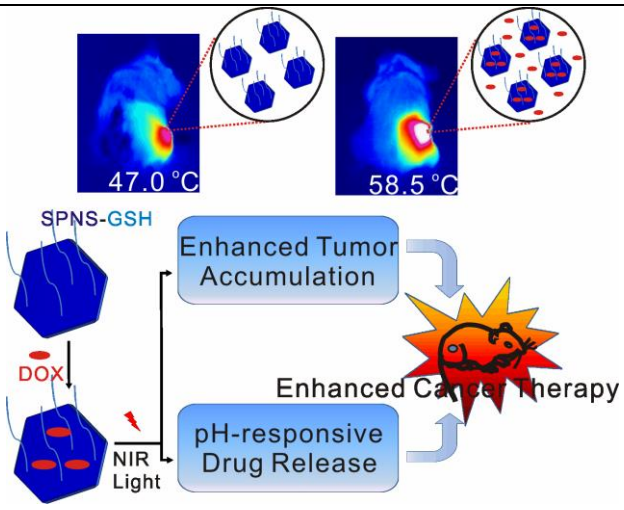

Enhanced cancer therapy is achieved by combining chemotherapy and enhanced photothermal therapy

Website for Nanfeng Zheng:
http://chem.xmu.edu.cn/groupweb/nfzheng/index.asp

Nano Research
DOI (automatically inserted by the publisher)
Research Article
ISSN 1998-0124
CN 11-5974/O4

Multifunctional Ultrasmall Pd Nanosheets for Enhanced Near-Infrared Photothermal Therapy and Chemotherapy of Cancer

Shaoheng Tang, Mei Chen, and Nanfeng Zheng (✉)

State Key Laboratory for Physical Chemistry of Solid Surfaces, Collaborative Innovation Center of Chemistry for Energy Materials, and Department of Chemistry, College of Chemistry and Chemical Engineering, Xiamen University, Xiamen 361005, China

Received: day month year
Revised: day month year
Accepted: day month year (automatically inserted by the publisher)

KEYWORDS
photothermal therapy,
chemotherapy,
Pd nanosheets,
drug delivery,
synergistic effect

ABSTRACT

NIR Photothermal therapy has developed very quickly in recent years. However, its clinical applications are hindered by the many practical problems, such as low accumulation in tumor, high laser power density and high biotoxicity *in vivo*. Herein, a versatile system combining chemotherapy with photothermal therapy for cancer therapy using ultra-small Pd nanosheet (SPNS) was developed. The SPNS can serve as pH-responsive drug carriers to efficiently deliver DOX into cancer cell and tumor. On the other hand, the coordinative loading of DOX on SPNS enhances its accumulation in tumor tissue. So we can efficiently ablate tumor using low-intensity laser radiation. Importantly, with ultra-small size (~4.4 nm), the GSHylated SPNS can be cleared from body through the renal into urine. The cancer therapeutic nanosystem, which exhibit a significant synergistic effect and low systemic toxicity, hold great potentials for clinical applications.

1 Instruction

Photothermal therapy using NIR laser has recently emerged as a new candidate technique for cancer treatment [1-3]. This technique involves absorbing the visible and near-infrared (NIR) light and converting it into heat [4]. NIR light is highly desirable for *in vivo* imaging and therapeutic applications owing to the minimal optical absorption of blood and soft tissue in this region to allow the maximal tissue penetration [5]. Many NIR resonant nanomaterials such as Au nanoshells [6], Au nanorods [7], Au nanocages [8], graphene nanosheets [9, 10], carbon nanotubes [11, 12] and Pd nanosheets [13], have been widely studied, because these nanomaterials can strongly absorb NIR light and convert it into cytotoxic heat upon remote NIR laser irradiation.

Address correspondence to nfzheng@xmu.edu.cn

Although significant progress has been made on the NIR photothermal therapy, there are still challenges to be addressed before its clinical applications [14-26]. For example, efficient area of the photothermal destruction of cancer cells is restricted by spot size of laser beam, resulting in a confined therapeutic area of cancer tissues. In many cases, relatively high laser power (e.g., 2-4 W/cm^2 for gold nanomaterials) is required to obtain sufficient heat to kill cancer cells [27-32]. Moreover, NIR resonant nanomaterials may cause high toxicity due to their low-level renal clearance and nonspecific high accumulation in the organs of the reticuloendothelial system (RES) (e.g. liver, spleen) after systematic administration [33, 34].

We demonstrate in this work a multifunctional nanosystem integrating chemotherapy and photothermal therapy together to overcome several limitations of currently available NIR photothermal therapeutic systems as discussed above. The system is based on ultra-small Pd nanosheets (SPNS) functionalized with anticancer drug doxorubicin hydrochloride (DOX). SPNS have an average diameter of ~4.4 nm, and thus exhibit both high photothermal efficiency and optimal clearance characteristics. DOX molecules are loaded on SPNS mainly through Pd-N coordination bonding. After the SPNS-DOX hybrid nanoparticles are surface-functionalized with reduced glutathione (GSH), the obtained SPNS-DOX-GSH composite exhibits the following synergistic properties for cancer therapy: 1) The coordinative loading of DOX on SPNS enhances its accumulation in tumor tissue, significantly reducing the laser power required to achieve effective tumor ablation; 2) SPNS can serve as pH-responsive drug carriers to efficiently DOX delivery. More importantly, the size of SPNS-DOX-GSH is well below the renal filtration size, allowing the therapeutic agents to be effectively cleared from bodies.

2 Experimental

2.1 Synthesis of 4.4 nm Palladium Nanosheets

Pd(II) acetylacetonate (Pd(acac)$_2$, 10.0 mg), poly(vinylpyrrolidone) (PVP, MW=30000, 32.0 mg) and NaBr (30.6 mg) were mixed together with N,N-Dimethylpropionamide (2 mL) and water (4 mL). After 10 hours on standing, the resulting homogeneous yellow solution was transferred to a glass pressure vessel. The vessel was then charged with CO to 1 bar and heated at 100 °C for 2 h before it was cooled to room temperature. The dark blue products were precipitated by acetone, separated via centrifugation and further purified by an ethanol-acetone mixture.

2.2 The loading of DOX to Pd nanosheets

0.5 mL solution of purified Pd nanosheets (200 μg mL^{-1}) was mixed with 0.5 mL DOX (1 mg mL^{-1}). The mixture was kept at 4 °C overnight before centrifugation. The particles were then washed with water at least 5 times and then dispersed in 5 mL RPMI 1640 culture medium.

2.3 Cancer cells culture and their incubation with Pd nanosheets.

Human hepatoma cells (QGY-7703) were cultured in RPMI 1640 medium in 24-well plates. The density was 1×10^5 cells/well. Before incubation with Pd nanosheets, the cells were seeded for 24 h. 0.5 mL of SPNS-DOX in culture medium were added to each well at a concentration of 20 μg mL^{-1}. The incubations were carried out at 37 °C in 5% CO_2 atmosphere for 12 h. After incubation, the cell medium was removed, and the cells were washed before PBS buffer solution was added.

2.4 Photothermal killing of cancer cells incubated with SPNS-DOX.

After incubation with SPNS-DOX, human hepatoma cells were exposed to a 1.4 W cm^{-2} 808-nm laser for 2 min to induce photothermal cell damage. To identify the cell viability, the dead cells were stained with Trypan Blue.

2.5 *In Vivo* Photothermal Destruction of Tumors.

4T1 murine breast cancer cells (cell storeroom of Chinese Academy of Science) was cultured in RPMI 1640 medium supplemented with 10% FBS and 1% penicillin/streptomycin (all reagents from Hyclone) under 5% CO_2 atomosphere. The 4T1 cells (2×10^6 cells)

were harvested, suspended in 50 μL PBS, and subcutaneously injected into the back of female Balb/c mice of each group (n=10). When the tumors were grown up to a volume of ~100 mm^3, the mice of each group were intravenously injected with 200 μL of each solution (1.5 mg mL^{-1} SPNS-GSH or SPNS-DOX-GSH solution, 0.085 mg mL^{-1} DOX solution, PBS) and irradiated with 0.3 W cm^{-2} continuous NIR laser to tumor region for 5 min 24 h after injection. The tumor size of each group was measured using a skinfold caliper, and tumor volume was calculated using the following equation: tumor volume=$ab^2/2$, where a is the maximum diameter of tumor and b is the minimum diameter of tumor. All studies on animals were done in accordance with the Guidelines for the Care and Use of Laboratory Animals in Fujian province, China.

2.6 Urine Excretion of Pd nanosheets

Male Sprague-Dawley rats (220 ± 30 g) were purchased from the Shanghai SLAC Laboratory Animal Co. Ltd. Rats were injected via the tail vein with 200 μL of PBS containing 300 μg of SPNS-DOX-GSH. Those rats were placed in stainless-steel metabolic cages and urine was collected. After collection of urine, samples of 1 mL digested by aqua regia and measured by ICP-MS.

2.7 ICP-MS analysis

Each tissue sample was completely digested by 2 mL of aqua regia at room temperature overnight. Subsequently, the solution was diluted to 10 mL using 0.5% HCl and 2% HNO_3. Samples were passed through a 0.22-mm filter to remove any undigested debris prior, and then subjected to ICP-MS measurements. The analysis of Pd content was performed on ICP-MS (PerkinElmer DRC- Ⅱ). Quantification was carried out by external five-point calibration with internal standard correction and the percentage of injected Pd dose per gram of tissue (%ID/g) was calculated.

3 Results and discussion

3.1 Characterization of SPNS-DOX

To fabricate the SPNS-DOX nanoparticles, uniform SPNS with the average diameter of ~4.4 nm (Fig. 1(a)) were first prepared by reducing Pd(II) acecylacetonate using CO as both reducing and shaping controlling agents. The loading of DOX was then performed by dispersing and stirring the SPNS in a solution of DOX. The SPNS were able to load up to about 5.3% of DOX through Pd-N coordination bonding (Fig. S1 in the Electronic Supplementary Material (ESM)). Similarly to the Pd nanosheets, the as-prepared SPNS-DOX exhibits the strong surface plasmon resonance (SPR) absorption in the NIR region (Fig. 1(b)).

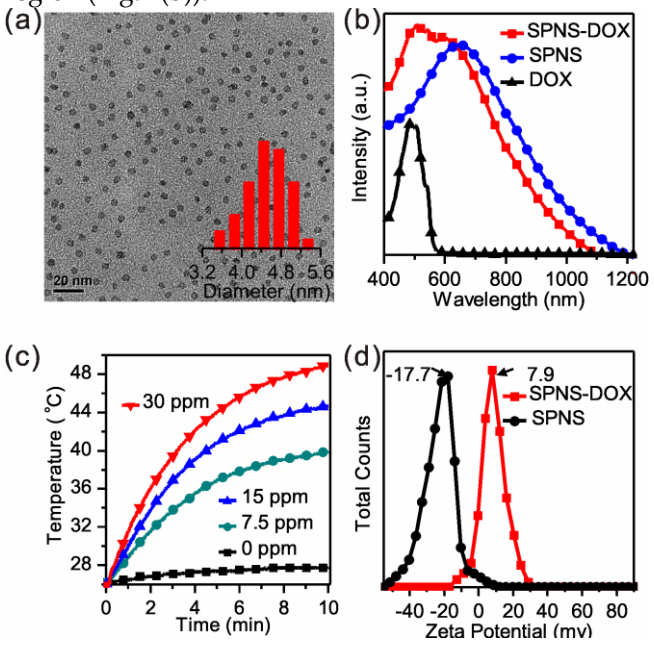

Figure 1 Characterization and NIR photothermal properties of SPNS-DOX. (a) TEM image of the SPNS. Inset: diameter distribution of the SPNS. (b) Absorption spectrum of the DOX, SPNS and SPNS-DOX. (c) Photothermal effect of SPNS-DOX. The temperature versus time plots were recorded for various concentrations of SPNS-DOX upon irradiation by a 1-W laser. (d) Zeta potential distributions of original SPNS and SPNS-DOX in the PBS buffer (pH = 7.4).

The photothermal effect of SPNS-DOX induced by the NIR SPR absorption was investigated by monitoring the temperature of 1 mL aqueous solutions of various concentration of SPNS-DOX (i.e., 0, 7.5, 15 and 30 ppm Pd) irradiated by a NIR laser (808 nm, 1 W at 0.35 cm^2). As shown in Fig. 1(c), the temperature of the SPNS-DOX solution containing 30 ppm Pd was risen from 25.6 to 48.8 °C after 10 min irradiation. Most importantly, after coated with DOX, the charge of the Pd nanosheets at pH=7.4 was shifted from -17.7 mV to +7.9 mV (Fig. 1(d)). It is well

known that the positively charged nanomaterials are more prone than negatively charged one to be taken up by living cells. Our ICP-MS measurements did confirm the enhanced cellular uptake of SPNS by the DOX modification (Fig. S2 in the ESM). This suggests that compared to SPNS, the SPNS-DOX should exhibit not only chemotherapeutic but also enhanced photothermal efficacy of cancer cells killing.

3.2 chemo-photothermal therapeutic efficacy of SPNS-DOX *in vitro*

To examine the effect of DOX loading on the overall chemo-photothermal therapeutic efficacy of SPNS-DOX, we first investigated the anticancer performances of SPNS-DOX *in vitro*. Human hepatoma cells (QGY-7703) were plated in 24-well plate and then further incubated in the medium containing desired concentration SPNS-DOX or free DOX for 12 h for comparison studies. Owing to the fluorescence of DOX (Fig. S3 in the ESM), it was possible to use fluorescence signals to quantitatively determine the amount of drug in cells by flow cytometry. As clearly illustrated in Fig. 2(a), after being loading on Pd nanosheets, DOX could be delivered into cells more efficiently. Moreover, DOX was released from SPNS-DOX in a pH-dependent manner. The release rate of DOX increased significantly with decreased pH (Fig. 2(b)). 3.0%, 17.0%, 42.8%, and 49.7% of the adsorbed DOX were released within 24 h in PBS buffer solutions of pH 7.4, 6.6, 5.2, and 3.6, respectively. It well known that cancer cells usually have a lower pH than normal cells [35, 36]. So it was expected that SPNS-DOX should release DOX faster in hepatoma cells than in hepatocytes (QSG-7701). To verify such an expectation, both cells were incubated with medium contain different concentrations of SPNS-DOX for 12 h. As shown in Fig. 2(c), SPNS-DOX indeed exhibits a higher cytotoxicity for hepatomas cells than hepatocytes as measured by standard MTT assay.

More interestingly, compared to SPNS, SPNS-DOX exhibits an enhanced photothermal therapy efficacy as well. As discussed above, the positive charged nature of SPNS-DOX is expected to facilitate the cellular uptake of Pd nanosheets, which should significantly enhance their efficacy in photothermal therapy of cancer cells. In our studies, after 12h incubation with SPNS or SPNS-DOX, QGY-7703 cells were irradiated by 808-nm laser at 1.4 W cm^{-2} to evaluate their therapeutic efficacies. As illustrated in Fig. 2(d), 100% of the cells incubated with SPNS-DOX were killed after 2 min irradiation. In comparison, at the same condition only half of the cells were killed by the unmodified SPNS (Fig. S4 in the ESM). Less than 20% cancer cells were killed by chemotherapy of SPNS-DOX in 12h. We therefore consider the enhanced cell killing efficacy SPNS-DOX was mainly because of the enhanced photothermal therapy.

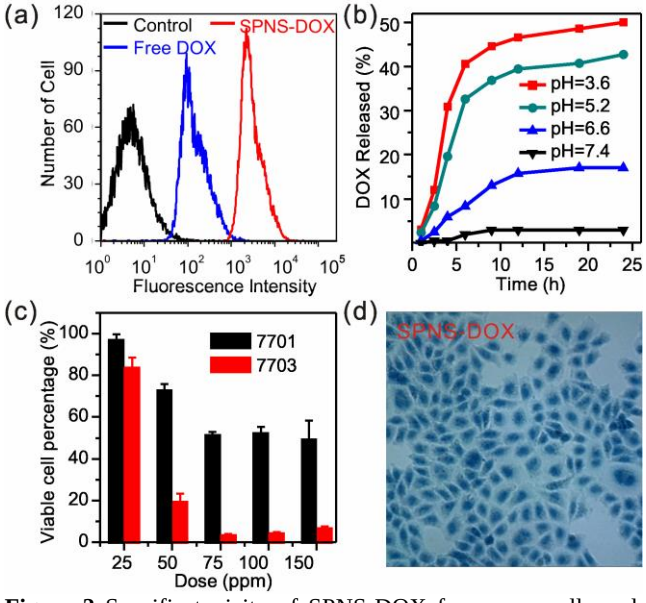

Figure 2 Specific toxicity of SPNS-DOX for cancer cells and enhanced photothermal therapy in vitro. (a) Flow cytometric profiles of QSG-7703 cells after being incubated with free DOX and SPNS-DOX. (b) pH-dependent releasing kinetics of DOX from SPNS-DOX. (c) Viability of healthy liver cells (QSG-7701) and hepatoma cells (QGY-7703) incubated for 12 h with different-concentrations of SPNS-DOX. The cell viabilities were measured by standard MTT assay. (d) Micrographs of QGY-7703 cells after 12 h incubation with SPNS-DOX and also 2 min irradiation of NIR laser (1.4 W cm^{-2}, 808 nm).

3.3 Blood circulation and biodistribution *in vivo*

The excellent *in vitro* chemo-photothermal therapeutic performances of SPNS-DOX have motivated us to further evaluate their behaviours in *in vivo* anticancer therapies. According to our previous study, the surface modifation by reduced glutathione (GSH) not only contributes to rendering the nanoparticles with desired stealthiness to the reticuloendothelial system (RES) organs, but also contributes to clearance of nanoparticles out of body by renal excretion. To modify SPNS-DOX with GSH,

0.5 mL DMF solution of SPNS-DOX (5 mg mL^{-1}) was added into 3 mL of GSH solution (1.0 mg mL^{-1}). The mixture was then shaken for 12 h at room temperature. Both SPNS-DOX samples before and after GSHylation were well dispersed in whole fetal bovine serum (FBS) and displayed nearly identical UV-Vis absorption profiles (Fig. S5 in the ESM).

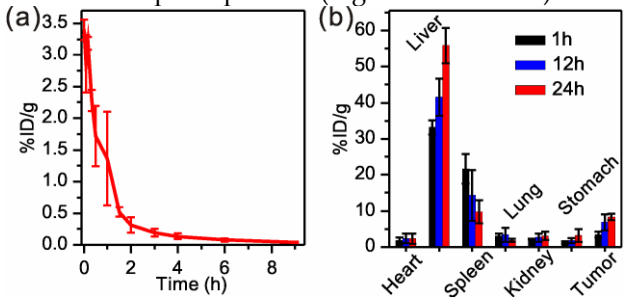

Figure 3 Pharmacokinetics and biodistribution of SPNS-DOX-GSH were studied by ICP-MS. (a) The blood circulation curve of SPNS-DOX-GSH determined by measuring Pd ion concentration in the blood at different time points post injection. (b) Biodistribution of SPNS-DOX-GSH in mice each organ. The unit was a percentage of injected dose per gram tissue (% ID/g). Error bars were based on triplicated samples.

In order to study the *in vivo* behaviors of SPNS-DOX-GSH, male Sprague-Dawley (SD) rats were first chosen as the animal model to study the blood circulation. After a surgical operation, SPNS-DOX-GSH at a dose of 1 mg kg^{-1} was infused via the jugular vein to three rats respectively [37]. Blood samples (approximately 0.4 mL) were drawn via the carotid artery at different time points after administration. The samples were then lysed by aqua regia and measured by inductively coupled plasma mass spectrometry (ICP-MS) to determine the Pd ion concentration in samples. The blood circulation curve showed that the pharmacokinetics of SPNS-DOX-GSH followed a two-compartment model with the first and second phase blood circulation half-lives of ~ 0.4 h and 1.5 h, respectively (Fig. 3(a)). To further investigate their biodistributions, the SPNS-DOX-GSH was injected into Balb/c mice bearing 4T1 tumors via tail vein. Mice were sacrificed at 1, 12 or 24 hours post injection (p.i.), and their major organs (n = 3 per group) were weighed and lysed by aqua regia. The obtained homogenized tissue lysates were diluted and measured by ICP-MS to quantitatively determine the Pd concentrations. Importantly, as shown in Fig. 3(b), a high tumor accumulation (~10% ID/g) was observed at 24h p.i.. In contrast, under the same operation condition, the accumulation of SPNS-GSH in tumor is ~6% ID/g (Fig. S6 in the ESM). These results indicated that DOX loading on SPNS-GSH was also beneficial to enhance accumulation of the photothermal agents in solid tumors.

3.4 Photothermal effect of SPNS-DOX-GSH *in vivo*

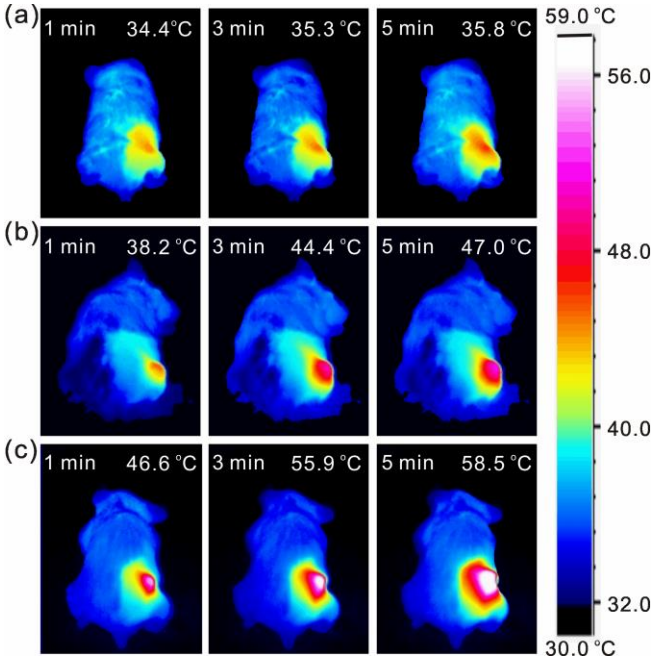

Figure 4 Photothermal effect in vivo. Infrared thermal imaging under the photothermal heating by 808-nm laser irradiation for different time periods in saline-injected (a), SPNS-GSH-injected (b) and SPNS-DOX-GSH-injected (c) tumor under 0.3 W cm^{-2} irradiation.

Encouraged by the high accumulation of SPNS in tumors and their strong NIR optical absorption, we then investigated the *in vivo* photothermal effect of SPNS-DOX-GSH by using NIR laser. The 4T1 tumor-bearing Balb/c mice were randomly divided into three groups (n = 3 per group) which were intravenously injected with 200 μL of saline, SPNS-GSH and SPNS-DOX-GSH in PBS (1.5 mg mL^{-1}), respectively. At 24-h p.i., the tumors were exposed to 808 nm laser at the density of 0.3 W cm^{-2} for 5 min. An infrared camera was used to record the full-body thermographic images (Fig. 4) and the temperature profile (Fig. S7 in the ESM). Under the

irradiation, for a typical mouse injected with SPNS-DOX-GSH, the tumor surface temperature increased rapidly from 32°C to reach 58.5°C within 5 min. In marked contrast, the tumor surface temperature of the groups injected with SPNS-GSH was increased to 47.0 °C at the same condition while the temperature for the one with saline was ramped to 35.8°C only. These results clearly demonstrated the enhanced accumulation of SPNS in tumors resulted from the DOX loading has dramatically improved the photothermal therapeutic efficacy of Pd nanosheets. Such an improvement allows the use of low-power NIR for the therapeutic purpose and thus makes the NIR photothermal therapy safer.

3.5 Chemo-photothermal therapeutic efficacy of SPNS-DOX *in vivo*

To further investigate the advantages of SPNS-DOX-GSH in chemo-photothermal cancer therapy *in vivo*, series of animal experiments were carried out using different materials. Balb/c mice were bilaterally injected in the hind flank with ~2×10^6 4T1 cells. After the tumor volume reached about 100 mm^3, the mice were randomly divided into seven groups (n = 5 per group). A group of five mice were intravenously injected with 200 μL of SPNS-DOX-GSH at 1.5 mg ml^{-1} (a dose of 300 μg) with tumors irradiated by the 808 nm laser for 5 min at a low power density of 0.3 W cm^{-2} at 24 h p.i.. The group was denoted as 'SDG + Laser'. For comparison, another group of five mice (denoted as the 'SG + Laser' group) were injected with SPNS-GSH at the same dose (300 μg) and exposed to the laser at the same conditions as used for 'SG + Laser'. In addition, another group of five mice (denoted as the 'D + SG + Laser' group) were injected with free DOX (17 μg) and SPNS-GSH (300 μg) and then exposed to the laser at the same conditions as used for 'D + SG + Laser'. Four other groups included saline injected mice (Control), saline injected mice exposed to laser (Laser), free DOX injected mice (denoted as "D") and SPNS-DOX-GSH injected mice without laser irradiation (denoted as 'SDG'), were also used as controls. The tumor sizes and mice survival were monitored every 2 days after treatments (Fig. 5(a,b)).

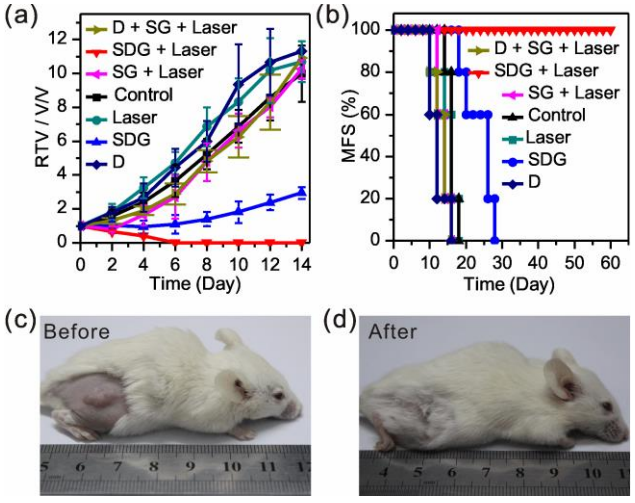

Figure 5 Photothermal destruction of tumors in mice using intravenously injected SPNS-DOX-GSH. (a) Relative Tumor Volume (RTV) of different groups after treatment. The tumor volumes were normalized to their initial sizes (n=5 per group). (b) Morbility Free Survival (MFS) curves of mice bearing 4T1 tumor after various treatments indicated. SPNS-DOX-GSH injected mice after photothermal therapy survived over 60 days without any single death. (c,d) Representative photographs of the mice before (c) and after (d) treatment. The laser irradiated tumors on SPNS-DOX-GSH injected mice were completely destructed.

As shown in Fig. 5(a), the mice treated only with free DOX (17 μg) exhibited rapid tumor volume increase. indicating that the dosage of administered DOX was too low to reduce the tumor volume. On the other hand, for the mice treated with SPNS-DOX-GSH ('SDG' group), the growth of tumors was inhibited only within the first four days in which slightly reduced tumor volumes were observed. However, beyond six days, the recurrence of tumor growth was observed with continuously increased tumor volume, suggesting that SPNS-GSH effectively deliver DOX into tumor but the tumors were not completely ablated in the 'SDG' group treated with only chemotherapy. Similarly, for the mice in the 'SG + Laser' group, the tumor growth was slightly inhibited only in the first two days after treatments, suggesting that the irradiation of 808 nm laser at 0.3 W cm^{-2} on SPNS-GSH nanosheets did not generate enough heat to ablate the tumor tissues, or even suppress their growth. However, All irradiated tumors on the mice in the 'SDG + Laser' group disappeared (Fig. 5(a)), leaving the original tumor sites with black scars which fell off in ~2 weeks after the treatments (Fig.5(c,d)). No tumor regrowth was noted in this treated group over a course of 60 days, after which the study was ended. In all the other four

groups (i.e., control, Laser, SG + Laser, D + SG + Laser), tumors grew rapidly after treatments. Interestingly, even the treatment of free DOX + SG + Laser can't effectively ablate tumors, suggesting that only the DOX loaded on the surface of SPNS-DOX could enhance the accumulation of the photothermal agent in the tumors to promote the efficacy of photothermal therapy *in vivo*.

All the results suggested that the chemotherapy and photothermal therapy were successfully combined in the SPNS-DOX-GSH nanosystem. The system exhibit an obvious synergistic effect that the combined DOX and photothermal treatments were more cytotoxic than chemotherapy or photothermal treatment alone. This synergistic effect was ascribed to enhanced cytotoxicity of DOX at elevated temperatures [38-40] and a higher accumulation of the SPNS-DOX-GSH in the tumor than SPNS-GSH.

It should be noted that the 'SDG + Laser' treatment indeed significantly increased the life spans of treated mice. The mice in the 'SDG + Laser' group were tumor-free after the treatment (SPNS-GSH injection, NIR laser irradiation) and survived over 60 days without a single death (Fig. 5(b)), while mice in the six control groups showed much shorter life spans averaged at 16-22 days. These comprehensive studies clearly demonstrated that SPNS-DOX-GSH was a powerful agent for combined chemotherapy and photothermal cancer therapy *in vivo*.

3.6 Clearance properties of SPNS-DOX-GSH *in vivo*

As revealed in both *in vitro* and *in vivo* studies, a significant synergistic effect to enhance both chemotherapy of DOX and photothermal therapy of Pd nanosheets was readily achieved by loading DOX on the photothermal agent, SPNS, the only inorganic components in our system, were serving as the NIR photothermal agent and the carriers for chemical drugs as well. What is also very important in the design of our system is that the size of Pd nanosheets is thoroughly below the renal filtration threshold (10 nm). The GSH-modified SPNS could be cleared out from bodies through the renal excretion route into urine. In this work, we also investigated the clearance properties of SPNS-DOX-GSH *in vivo*. Doses of 300 μg of SPNS-DOX-GSH were intravenously administered into male SD rats (n = 3). Urine was collected within a 15-day period after administration and Pd concentrations were measured by ICP-MS. As shown in Fig. 6, more than 7.4% of the SPNS-DOX-GSH were excreted out of the body within 1 day p.i. and up to 44.3% after 15 day p.i.. To assess the systematic toxicity of our combined therapeutic agent, mice treated with SPNS-DOX-GSH (300 μg) were evaluated by pathological examinations. Major organs of saline or SPNS-DOX-GSH + laser treated mice were collected for histology analysis 40 days after treatment. No noticeable lesions were observed from HE stained organ slices in organs of the treatment group (Fig. S8 in the ESM). Moreover, during the study, neither death nor significant body weight drop was noted in the SPNS-DOX-GSH + laser treated group (Fig. S9 in the ESM). These results indicated low systematic toxicity of SPNS-DOX-GSH *in vivo*.

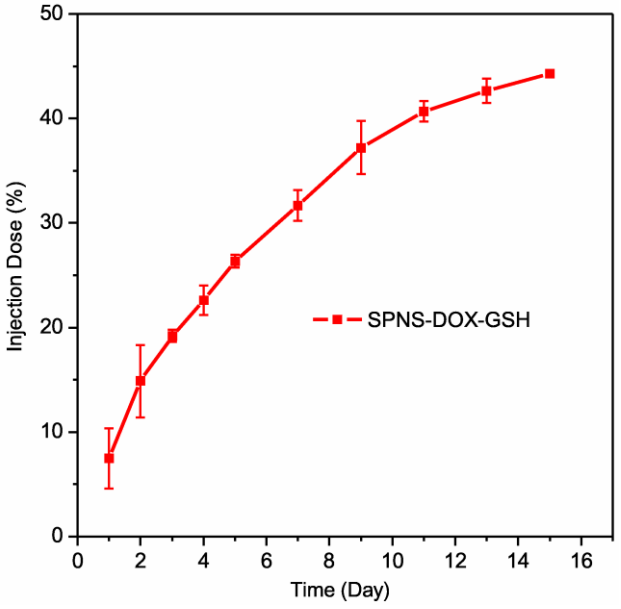

Figure 6 *In vivo* clearance of SPNS-DOX-GSH. Urinary cumulative excretion of SPNS-DOX-GSH in rats (n=3) following i.v. administration at a single dose of 10 mg kg^{-1}. The amount of Pd in urinary samples was measured by ICP-MS.

4 Conclusions

In summary, an effective cancer therapeutic nanosystem based on plasmonic ultrasmall Pd nanosheets was developed. With the Pd nanosheets as both the NIR photothermal agent and drug carriers for anticancer chemical drug (DOX), the developed nanosystem exhibited a significant synergistic effect to enhance both chemotherapy of

the chemical drugs and the photothermal therapy of the drug carriers. *In vitro* and *in vivo* studies clearly demonstrated that the loading of DOX improved the accumulation of Pd nanosheets in tumors and also optimized their uptakes by cancer cells. The synergistic effect allowed lower the dose of chemical drugs and the power of NIR laser for effective anticancer therapy. More importantly, due to the ultra-small size, the developed Pd-DOX-GSH hybrid nanoparticles were readily cleared from body through the renal excretion route and into urine. The chemo-photothermal therapeutic nanosystem demonstrated in this work hold great potentials for clinical applications.

Acknowledgements

We thank Prof. Xuan Zhu and Ms. Meiqin Su at Xiamen University for helping the animal experiment technique. This work was supported by the Ministry of Science and Technology of China (2011CB932403, 2014CB932004), the National Natural Science Foundation of China (21131005).

Electronic Supplementary Material: Supplementary material (please give brief details, e.g., further details of the annealing and oxidation procedures, STM measurements, AFM imaging and Raman spectroscopy measurements) is available in the online version of this article at http://dx.doi.org/10.1007/s12274-***-****-* (automatically inserted by the publisher).

References

[1] Lal, S.; Clare, S. E.; Halas, N. J. Nanoshell-Enabled Photothermal Cancer Therapy: Impending Clinical Impact. *Acc. Chem. Res.* **2008**, *41*, 1842-1851.

[2] Melancon, M. P.; Zhou, M.; Li, C. Cancer Theranostics with Near-Infrared Light-Activatable Multimodal Nanoparticles. *Acc. Chem. Res.* **2011**, *44*, 947-956.

[3] Huang, X.; Jain, P. K.; El-Sayed, I. H.; El-Sayed, M. A. Plasmonic photothermal therapy (PPTT) using gold nanoparticles. *Lasers Med. Sci.* **2008**, *23*, 217-228.

[4] Jain, P. K.; El-Sayed, I. H.; El-Sayed, M. A. Au nanoparticles target cancer. *Nano Today* **2007**, *2*, 18-29.

[5] Weissleder, R. A clearer vision for in vivo imaging. *Nat. Biotech.* **2001**, *19*, 316-317.

[6] Oldenburg, S. J.; Averitt, R. D.; Westcott, S. L.; Halas, N. J. Nanoengineering of optical resonances. *Chem. Phys. Lett.* **1998**, *288*, 243-247.

[7] Huang, X.; Neretina, S.; El-Sayed, M. A. Gold Nanorods: From Synthesis and Properties to Biological and Biomedical Applications. *Adv. Mater.* **2009**, *21*, 4880-4910.

[8] Chen, J.; Glaus, C.; Laforest, R.; Zhang, Q.; Yang, M.; Gidding, M.; Welch, M. J.; Xia, Y. Gold Nanocages as Photothermal Transducers for Cancer Treatment. *Small* **2010**, *6*, 811-817.

[9] Yang, K.; Zhang, S.; Zhang, G. X.; Sun, X. M.; Lee, S. T.; Liu, Z. Graphene in Mice: Ultrahigh In Vivo Tumor Uptake and Efficient Photothermal Therapy. *Nano Lett.* **2010**, *10*, 3318-3323.

[10] Sun, X.; Liu, Z.; Welsher, K.; Robinson, J. T.; Goodwin, A.; Zaric, S.; Dai, H. Nano-Graphene Oxide for Cellular Imaging and Drug Delivery. *Nano Res.* **2008**, *1*, 203-212.

[11] Moon, H. K.; Lee, S. H.; Choi, H. C. In Vivo Near-Infrared Mediated Tumor Destruction by Photothermal Effect of Carbon Nanotubes. *ACS Nano* **2009**, *3*, 3707-3713.

[12] Liu, Z.; Tabakman, S.; Sherlock, S.; Li, X.; Chen, Z.; Jiang, K.; Fan, S.; Dai, H. Multiplexed five-color molecular imaging of cancer cells and tumor tissues with carbon nanotube Raman tags in the near-infrared. *Nano Res.* **2010**, *3*, 222-233.

[13] Huang, X. Q.; Tang, S. H.; Mu, X. L.; Dai, Y.; Chen, G. X.; Zhou, Z. Y.; Ruan, F. X.; Yang, Z. L.; Zheng, N. F. Freestanding palladium nanosheets with plasmonic and catalytic properties. *Nat. Nanotech.* **2011**, *6*, 28-32.

[14] Kam, N. W. S.; O'Connell, M.; Wisdom, J. A.; Dai, H. J. Carbon nanotubes as multifunctional biological transporters and near-infrared agents for selective cancer cell destruction. *P. Natl. Acad. Sci. U S A* **2005**, *102*, 11600-11605.

[15] Hessel, C. M.; P. Pattani, V.; Rasch, M.; Panthani, M. G.; Koo, B.; Tunnell, J. W.; Korgel, B. A. Copper Selenide Nanocrystals for Photothermal Therapy. *Nano Lett.* **2011**, *11*, 2560-2566.

[16] Gobin, A. M.; Lee, M. H.; Halas, N. J.; James, W. D.; Drezek, R. A.; West, J. L. Near-Infrared Resonant Nanoshells for Combined Optical Imaging and Photothermal Cancer Therapy. *Nano Lett.* **2007**, *7*, 1929-1934.

[17] Tian, B.; Wang, C.; Zhang, S.; Feng, L.; Liu, Z. Photothermally Enhanced Photodynamic Therapy Delivered by Nano-Graphene Oxide. *ACS Nano* **2011**, *5*, 7000-7009.

[18] Liu, H.; Chen, D.; Li, L.; Liu, T.; Tan, L.; Wu, X.; Tang, F. Multifunctional Gold Nanoshells on Silica Nanorattles: A Platform for the Combination of Photothermal Therapy and Chemotherapy with Low Systemic Toxicity. *Angew. Chem. Int. Ed.* **2011**, *50*, 891-895.
[19] Yavuz, M. S.; Cheng, Y.; Chen, J.; Cobley, C. M.; Zhang, Q.; Rycenga, M.; Xie, J.; Kim, C.; Song, K. H.; Schwartz, A. G.; Wang, L. V.; Xia, Y. Gold nanocages covered by smart polymers for controlled release with near-infrared light. *Nat. Mater.* **2009**, *8*, 935-939.
[20] Huang, X.; El-Sayed, I. H.; Qian, W.; El-Sayed, M. A. Cancer Cell Imaging and Photothermal Therapy in the Near-Infrared Region by Using Gold Nanorods. *J. Am. Chem. Soc.* **2006**, *128*, 2115-2120.
[21] Tang, S. H.; Huang, X. Q.; Zheng, N. F. Silica coating improves the efficacy of Pd nanosheets for photothermal therapy of cancer cells using near infrared laser. *Chem. Commun.* **2011**, *47*, 3948-3950.
[22] Robinson, J. T.; Tabakman, S. M.; Liang, Y.; Wang, H.; Sanchez Casalongue, H.; Vinh, D.; Dai, H. Ultrasmall Reduced Graphene Oxide with High Near-Infrared Absorbance for Photothermal Therapy. *J. Am. Chem. Soc.* **2011**, *133*, 6825-6831.
[23] Huang, X. Q.; Tang, S. H.; Yang, J.; Tan, Y. M.; Zheng, N. F. Etching Growth under Surface Confinement: An Effective Strategy To Prepare Mesocrystalline Pd Nanocorolla. *J. Am. Chem. Soc.* **2011**, *133*, 15946-15949.
[24] Yang, G.; Gong, H.; Qian, X.; Tan, P.; Li, Z.; Liu, T.; Liu, J.; Li, Y.; Liu, Z. Mesoporous Silica Nanorods Intrinsically Doped with Photosensitizers as a Multifunctional Drug Carrier for Combination Therapy of Cancer. *Nano Res.* **2014**, 10.1007/s12274-014-0558-0.
[25] Wang, N.; Zhao, Z.; Lv, Y.; Fan, H.; Bai, H.; Meng, H.; Long, Y.; Fu, T.; Zhang, Z.; Tan, W. Gold nanorod-photosensitizer conjugate with extracellular pH-driven tumor targeting ability for photothermal/photodynamic therapy. *Nano Res.* **2014**, *7*, 1291-1301.
[26] Terentyuk, G.; Panfilova, E.; Khanadeev, V.; Chumakov, D.; Genina, E.; Bashkatov, A.; Tuchin, V.; Bucharskaya, A.; Maslyakova, G.; Khlebtsov, N.; Khlebtsov, B. Gold nanorods with a hematoporphyrin-loaded silica shell for dual-modality photodynamic and photothermal treatment of tumors in vivo. *Nano Res.* **2014**, *7*, 325-337.
[27] von Maltzahn, G.; Park, J.-H.; Agrawal, A.; Bandaru, N. K.; Das, S. K.; Sailor, M. J.; Bhatia, S. N. Computationally Guided Photothermal Tumor Therapy Using Long-Circulating Gold Nanorod Antennas. *Cancer Res.* **2009**, *69*, 3892-3900.
[28] Dickerson, E. B.; Dreaden, E. C.; Huang, X.; El-Sayed, I. H.; Chu, H.; Pushpanketh, S.; McDonald, J. F.; El-Sayed, M. A. Gold nanorod assisted near-infrared plasmonic photothermal therapy (PPTT) of squamous cell carcinoma in mice. *Cancer Lett.* **2008**, *269*, 57-66.
[29] Hirsch, L. R.; Stafford, R. J.; Bankson, J. A.; Sershen, S. R.; Rivera, B.; Price, R. E.; Hazle, J. D.; Halas, N. J.; West, J. L. Nanoshell-mediated near-infrared thermal therapy of tumors under magnetic resonance guidance. *P. Natl. Acad. Sci. U S A* **2003**, *100*, 13549-13554.
[30] Chen, J.; Wang, D.; Xi, J.; Au, L.; Siekkinen, A.; Warsen, A.; Li, Z.-Y.; Zhang, H.; Xia, Y.; Li, X. Immuno Gold Nanocages with Tailored Optical Properties for Targeted Photothermal Destruction of Cancer Cells. *Nano Lett.* **2007**, *7*, 1318-1322.
[31] O'Neal, D. P.; Hirsch, L. R.; Halas, N. J.; Payne, J. D.; West, J. L. Photo-thermal tumor ablation in mice using near infrared-absorbing nanoparticles. *Cancer Lett.* **2004**, *209*, 171-176.
[32] Tong, L.; Wei, Q.; Wei, A.; Cheng, J.-X. Gold Nanorods as Contrast Agents for Biological Imaging: Optical Properties, Surface Conjugation and Photothermal Effects†. *Photochem. and Photobiol.* **2009**, *85*, 21-32.
[33] De Jong, W. H.; Hagens, W. I.; Krystek, P.; Burger, M. C.; Sips, A. J. A. M.; Geertsma, R. E. Particle size-dependent organ distribution of gold nanoparticles after intravenous administration. *Biomaterials* **2008**, *29*, 1912-1919.
[34] Semmler-Behnke, M.; Kreyling, W. G.; Lipka, J.; Fertsch, S.; Wenk, A.; Takenaka, S.; Schmid, G.; Brandau, W. Biodistribution of 1.4- and 18-nm Gold Particles in Rats. *Small* **2008**, *4*, 2108-2111.
[35] Gerweck, L. E. Tumor pH: implications for treatment and novel drug design. *Semin. Radiat. Oncol.* **1998**, *8*, 176-182.
[36] Wike-Hooley, J. L.; Haveman, J.; Reinhold, H. S. The relevance of tumour pH to the treatment of malignant disease. *Radiother. Oncol.* **1984**, *2*, 343-366.
[37] Kim, S. H.; Choi, Y. M.; Lee, M. G. Pharmacokinetics and pharmacodynamics of furosemide in protein-calorie malnutrition. *Pharmacokinet. Biopharm.* **1993**, *21*, 1-17.
[38] Johnson, H. A.; Pavelec, M. Thermal enhancement of thio-TEPA cytotoxicity. *J. Natl.*

Cancer Inst. **1973**, *50*, 903-908.
[39] Hahn, G. M.; Braun, J.; Har-Kedar, I. Thermochemotherapy: synergism between hyperthermia (42-43 degrees) and adriamycin (of bleomycin) in mammalian cell inactivation. *P. Natl. Acad. Sci. U S A* **1975**, *72*, 937-940.
[40] Overgaard, J. Combined adriamycin and hyperthermia treatment of a murine mammary carcinoma in vivo. *Cancer Res.* **1976**, *36*, 3077-3081.

Electronic Supplementary Material

Multifunctional Ultrasmall Pd Nanosheets for Enhanced Near-Infrared Photothermal Therapy and Chemotherapy of Cancer

Shaoheng Tang, Mei Chen, and Nanfeng Zheng (✉)

State Key Laboratory for Physical Chemistry of Solid Surfaces, Collaborative Innovation Center of Chemistry for Energy Materials, and Department of Chemistry, College of Chemistry and Chemical Engineering, Xiamen University, Xiamen 361005, China

Supporting information to DOI 10.1007/s12274-**-****-* (automatically inserted by the publisher)**

Materials

$Pd(acac)_2$ (99%) and N,N-Dimethylpropionamide (DMP) was purchased from Alfa Aesar. PVP (MW=30000, AR) and sodium bromide were purchased from Sinopharm Chemical Reagent Co. Ltd. (Shanghai, China). Doxorubicin Hydrochloride was purchased from Beijing HuaFeng United Technology CO., Ltd. Male Sprague-Dawley rats (220 ± 30 g) and Balb/c mice were purchased from the Shanghai SLAC Laboratory Animal Co. Ltd. Human hepatoma cells (QGY-7703) were purchased from cell storeroom of Chinese Academy of Science. RPMI 1640 cell culture medium, bovine serum albumin (BSA) and Penicillin-Streptomycin compound were purchased from Hyclone Laboratories Inc. MTT was purchased from Sigma. The water used in all experiments was ultrapure. All reagents were used as received without further purification.

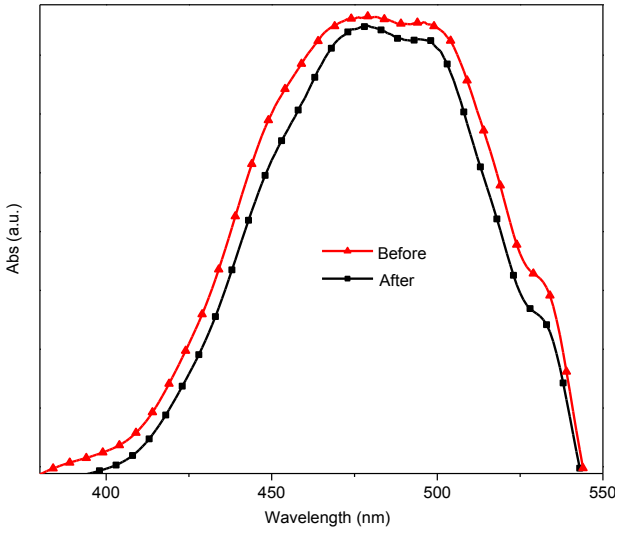

Figure S1 Absorption spectra of DOX solution before and after loading on SPNS.

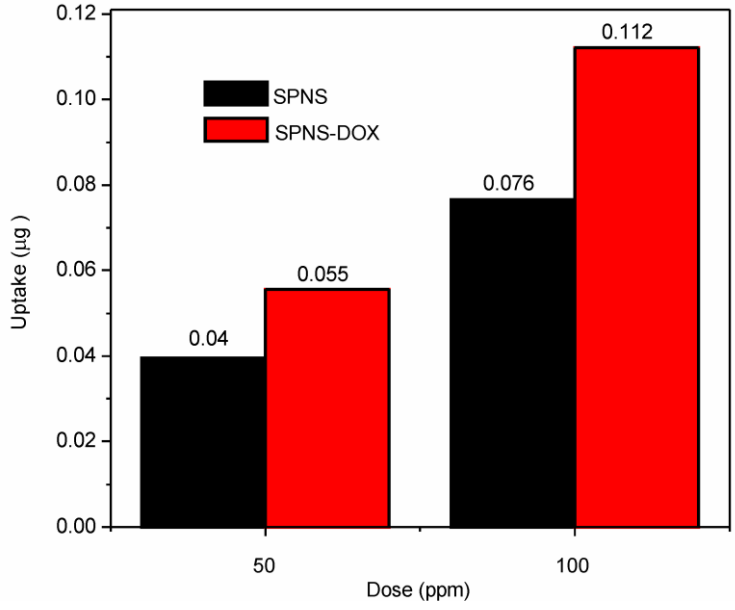

Figure S2 The uptake of SPNS before and after the loading of DOX as measured by ICP-MS.

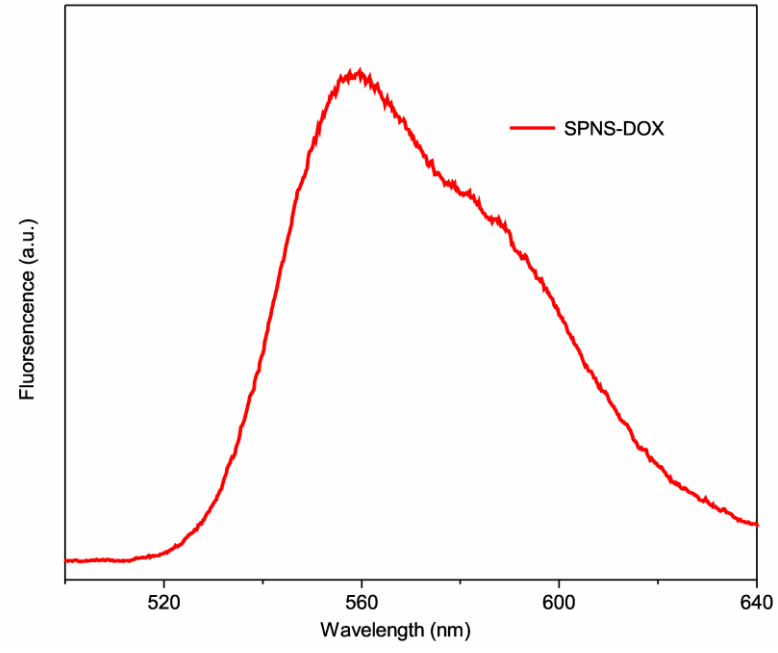

Figure S3 The fluorescence spectra of SPNS-DOX.

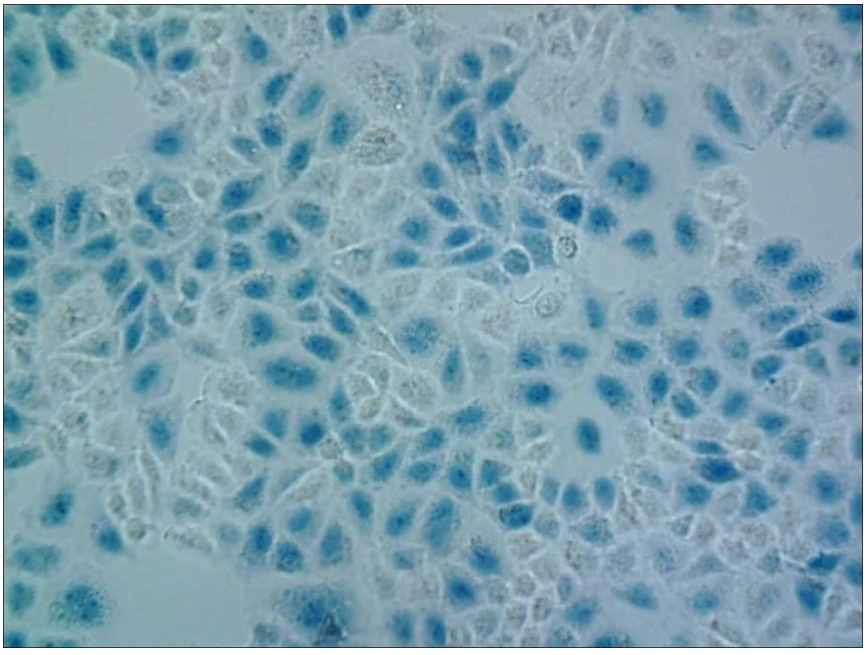

Figure S4 Micrograph corresponding to in vitro photothermal therapy by SPNS at an optical power density of 1.4 w cm^{-2}. Dead cells were stained with Trypan blue.

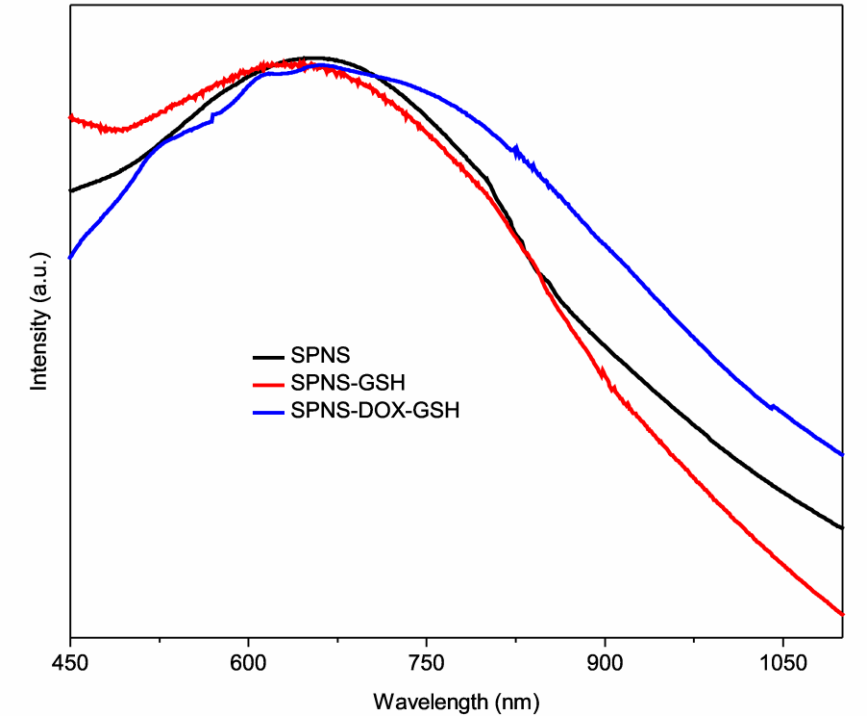

Figure S5 The absorption spectra of SPNS, SPNS-GSH and SPNS-DOX-GSH in FBS.

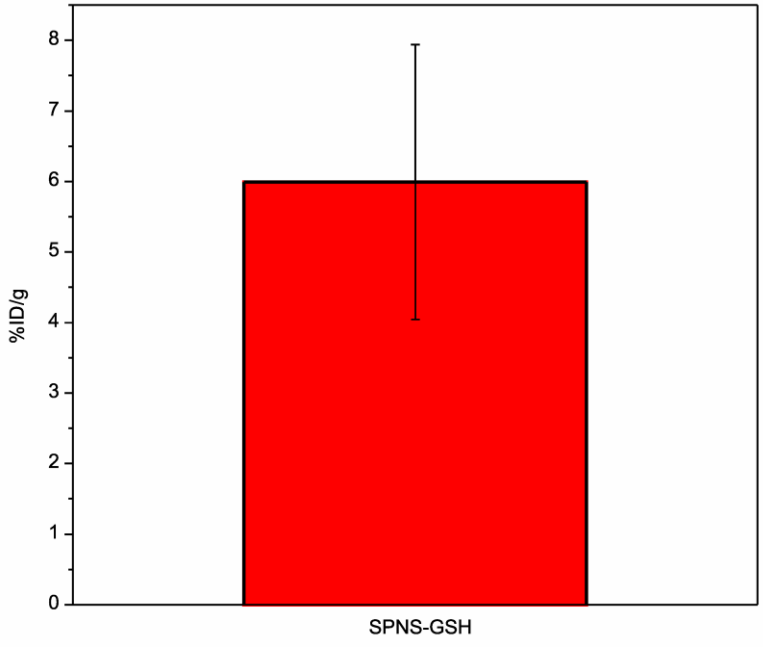

Figure S6 The accumulation of SPNS-GSH in tumor.

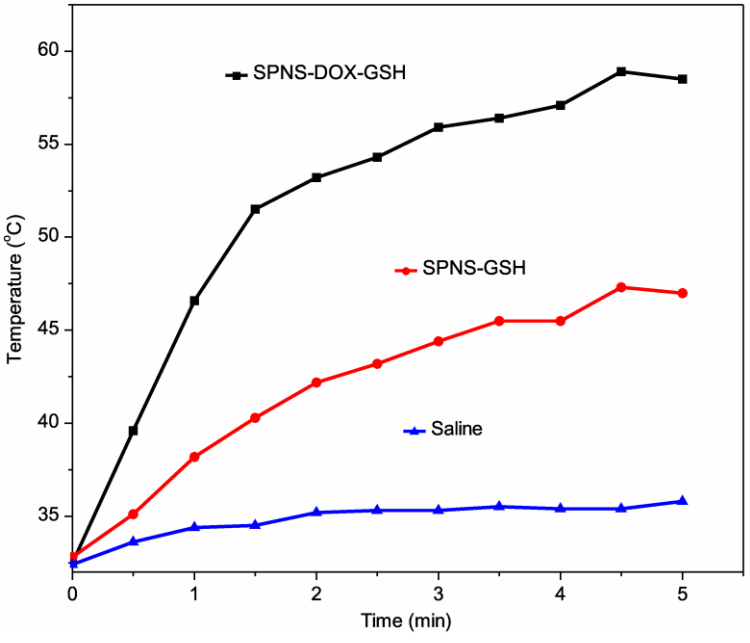

Figure S7 The temperature evolution on tumors of mice with SPNS-GSH, SPNS-DOX-GSH and saline injection. The tumors were exposed to the 808 nm laser at a power density of 0.3 W $cm^{-2.}$

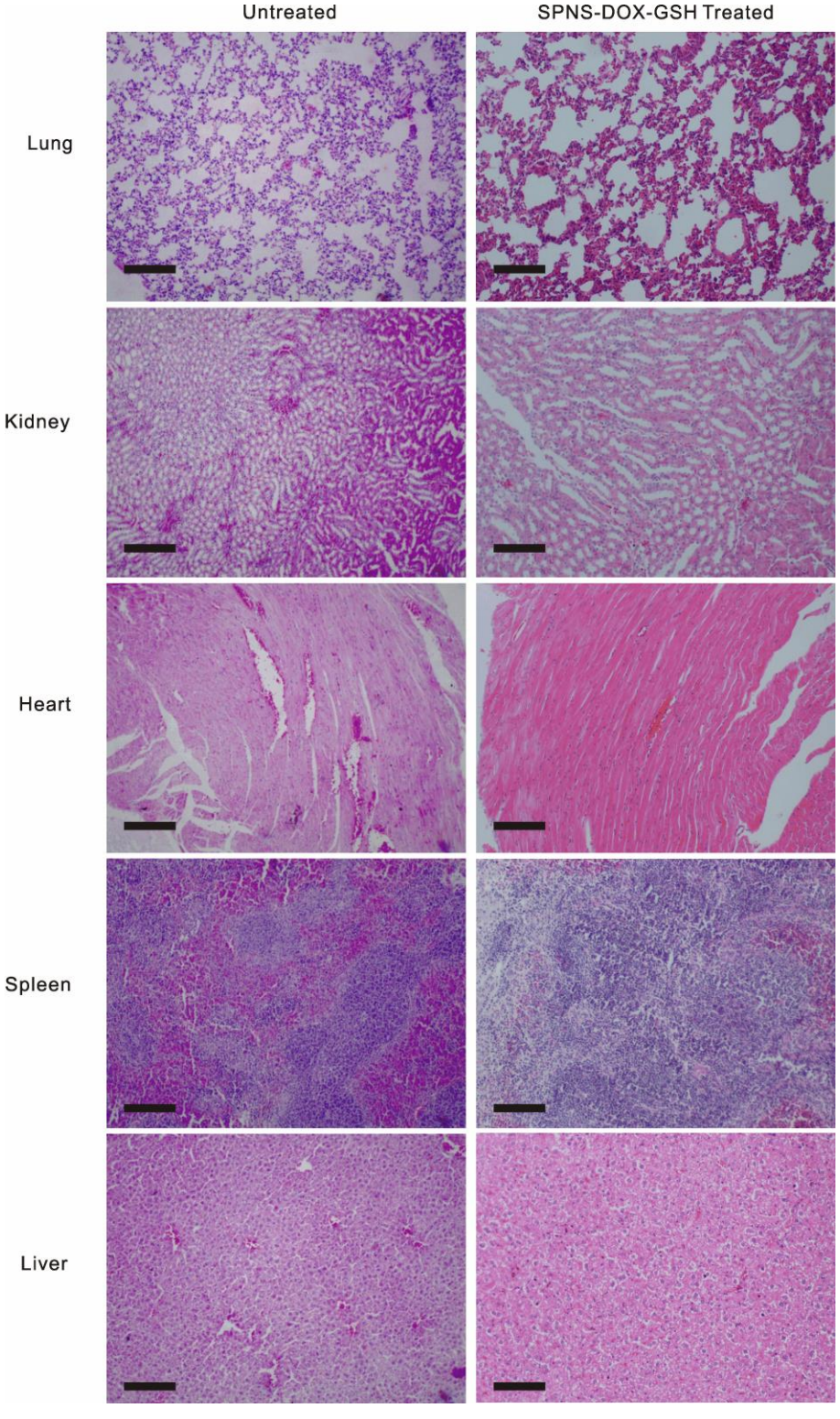

Figure S8 Major organs H&E stained images from untreated mice and mice survived after photothermal therapy. Scale bar: 100 μm.

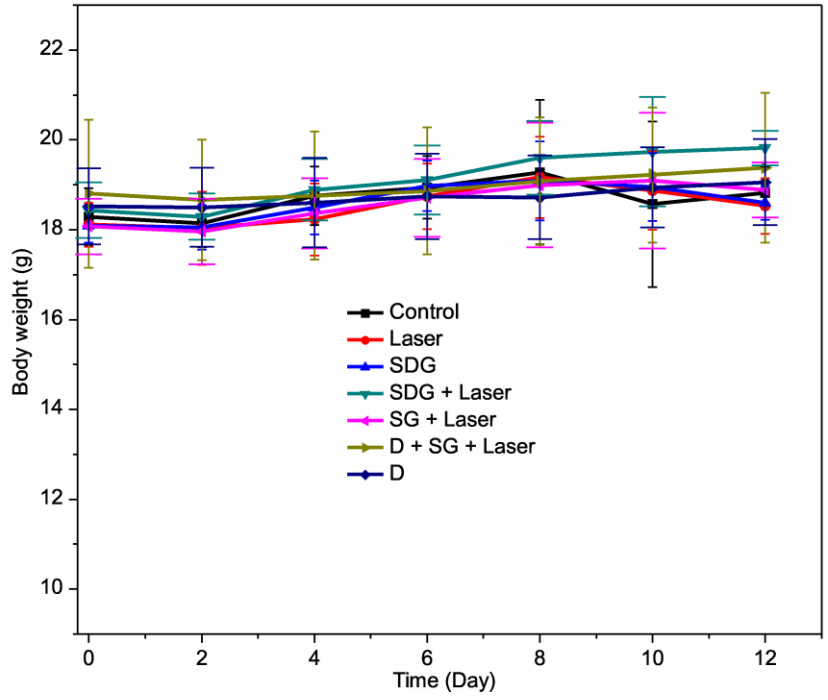

Figure S9 The body weight curves after various treatments.

Address correspondence to nfzheng@xmu.edu.cn